4

Identifying and Monitoring Evolving AE Sources

Rúnar Unnþórsson
University of Iceland
Iceland

1. Introduction

Fatigue is a stochastic process influenced by several random factors such as material, manufacturing and in-service variations. Due to the uncertainties involved, the true system cannot be accurately represented by a mathematical fatigue model. By combining condition monitoring techniques with fatigue modelling, critical material degradation processes can be identified, failure predicted, and preventive actions planned. This approach is known as condition-based maintenance. However, by using effective condition based maintenance, instead of corrective (after failure) or preventive (calendar-based) maintenance, substantial savings can be made. The savings will be in the form of extended part life, reduced number of unexpected breakdowns, lower risk of secondary failure, and increased safety.

Recent years have seen an increasing interest in the use of carbon fibres for applications in the automotive, aerospace and biomedical industries. Their popularity stems largely from their advantageous material properties such as high strength-to-weight ratio, fatigue strength, corrosion and heat resistance. Despite these properties, damage in Carbon Fibre-Reinforced Polymer (CFRP) composites develops early in service (Degrieck & Paepegem, 2001; Dzenis & Qian, 2001; Halverson et al., 1997) and continues to accumulate throughout the service life. The fatigue tolerance can be attributed to resistance to inhomogeneous damage growth, which is a property of highly inhomogeneous materials (Halverson et al., 1997). The high damage tolerance of composites means that composites are able to meet their in-service requirements for a prolonged period of time while damages accumulate and grow. Consequently, there is a definite advantage in being able to detect, monitor and evaluate individual damage mechanisms before the failure of a composite.

Acoustic Emission can be used to detect delamination, matrix cracking, debonding, fibre cracking and fibre pull-out (Giordano et al., 1998; Green, 1998; Nayeb-Hashemi et al., 1999; Tsamtsakis et al., 1998; Wevers, 1997). However, the high sensitivity of the AE technique means that the measured AE signal may contain a high number of AE transients from sources located both in the composite and the environment. The sources in the composite include damage growth, rubbing of crack surfaces and friction between the fibres and the matrix due to their different material properties. The varying material properties will result in an anisotropic speed of propagation (Duesing, 1989). In addition, reflection and attenuation of the AE waves add to the complexity. Attenuation can be caused by geometric spreading, dispersion, internal friction and scattering (Prosser, 1996). Furthermore, the AE waves from damage growth can be buried in the AE generated by the friction and rubbing of

crack surfaces (Mouritz, 2003). As a result, multiple AE transients with varying amplitude, duration, and frequency can be emitted simultaneously. Furthermore, the values of the AE signal features from cumulated damage usually fall in the same range as those that result from damage growth (Dzenis & Qian, 2001; Tsamtsakis et al., 1998).

An intuitive approach to condition monitoring using AE signals is to keep track of one or more waveform parameters, which characterize the AE from the source of interest. Each parameter, however, will follow a probability distribution, which changes when the source (damage) changes. Because of the parameter fluctuations and the high rate of AE with similar parameter values, waveform parameters alone are not sufficient for distinguishing between sources. Additional indication is therefore needed. For an example, if an AE source always emits an AE at the same load level, then the load level of AE occurrence is sufficient to distinguish between the sources. However, when a source evolves, e.g. a growing delamination crack, the load level of AE occurrence changes.

This chapter presents a methodology for processing, presenting, and quantifying AE data. It was designed for the purpose of identifying and tracking locations of multiple evolving AE sources in CRFP subjected to cyclic loading using a cyclic reference signal. The methodology can also be used for normal AE health monitoring of materials/machinery and is neither limited to AE signals nor to periodic reference signals. The chapter also presents an AE hit pattern feature which is made by fusing and coding AE hit-based features with timing information, i.e. the inter-spike intervals (ISI). The methodology was presented in (Unnthorsson et al., 2007a) and the feature was studied in (Unnthorsson et al., 2007b; 2008b).

The remaining of the chapter is organized as follows. Sections 2 and 3 introduce and explain, respectively, the methodology and the AE hit pattern feature. Then, an experimental case study is presented in section 4 and in section 5 both the methodology and the AE hit pattern feature are illustrated using the experimental data. Finally, section 6 concludes this chapter and suggests future research topics.

2. Monitoring evolving AE sources

In order to identify evolving AE sources in a signal which contains high AE activity from many different sources, e.g. evolving damages, non-evolving damages, friction, machinery and more, a set of procedures and signal processing methods need to be combined. In this section a methodology for this purpose is introduced. By using this methodology one can identify and locate interesting AE signals for further study, or for tracking, which otherwise would be difficult to accomplish due to the overwhelming number of sources with similar characteristics. Figure 1 shows a schematic overview of the methodology. It is divided into four steps which will be described and discussed in this section. The four steps are: segmentation, band-pass filtering, feature extraction and visualization.

2.1 First step: segmentation

Most professional AE systems offer the possibility of acquiring external parameters such as pressure, strain, load and displacement. If these parameters, or reference signals, are acquired simultaneously with the AE then any of them can be used as reference signals. By segmenting the AE signal so that all segments are exactly one cycle, of equal length and start at the same

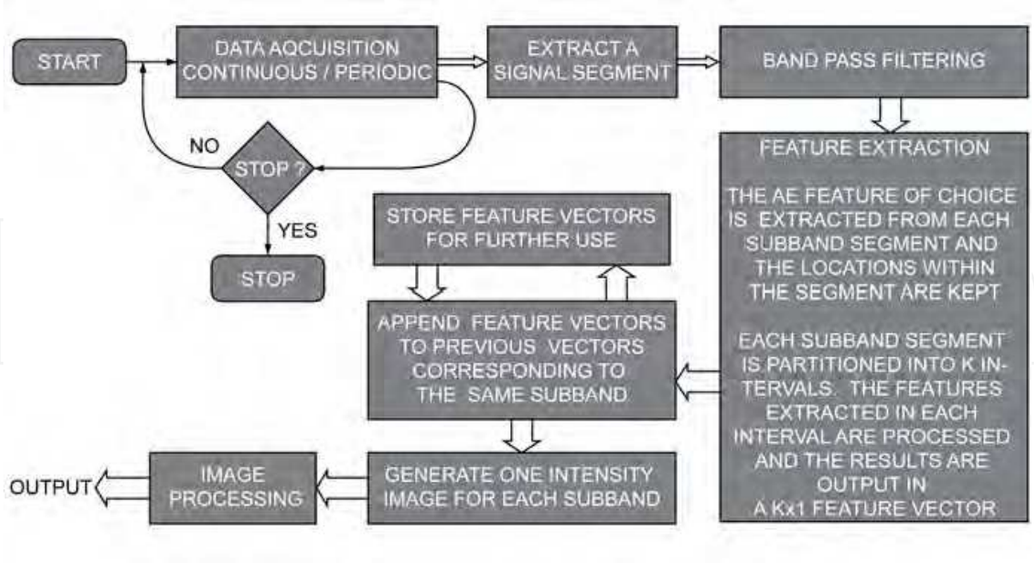

Fig. 1. Schematic overview of the methodology.

reference point of the reference signal then it is possible to compare segments and identify and monitor evolving AE sources. The segmentation, illustrated on the left side of in Fig. 2, can be applied to both periodic and aperiodic signals.

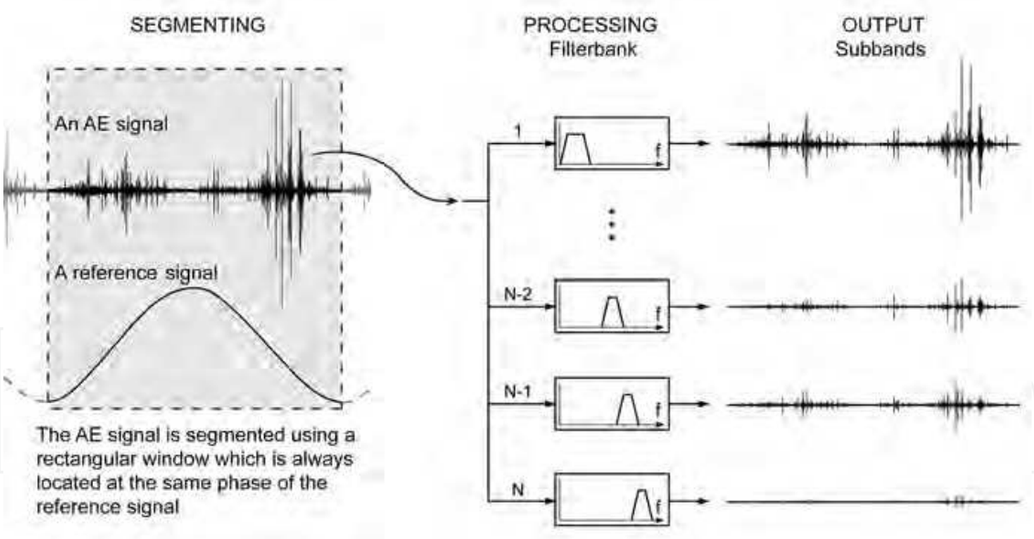

Fig. 2. Illustration of how the AE signal is segmented using a reference signal and then split into N subands. All segments start at the same phase of the reference signal and are exactly one cycle.

2.2 Second step: Band-pass filtering

Multi-resolution analysis of AE signals is a valuable tool for identifying band-limited AE sources. This is because AE from different damage mechanisms resides in frequency

bands (Bohse, 2000; De Groot et al., 1995; Iwamoto et al., 1999; Kamala et al., 2001). Hence, the subband filtering can enable detection of sources which otherwise could be masked out and left undetected. The decomposition of each segment, s, into N subbands is illustrated on the right side of Fig. 2.

Several methods are available for decomposing the AE signal into subbands. The selection of the method, the type of filters used, the number of subbands (N) and the bandwidth of each subband, depends on the user and his preferences. Two methods are mentioned here; a filter bank representation of the discrete wavelet transform and a method known as phaseless filtering (Mercer, 2001).

The filter bank representation of the discrete wavelet transform (DWT) offers a convenient method for decomposing the AE signal into subbands. In the filter bank, the conventional discrete wavelet decomposition, at each level, is computed by filtering the input signal with low and high pass filters, producing two sequences, and keeping only their even numbered coefficieFnts. All subsequences of the original signal are called wavelet packets, and together they form a wavelet packet tree. Each packet retains the necessary information in order to reconstruct the signal in the corresponding subband. This means that packets from different levels can be used to fully reconstruct the original signal if, together, they span the full bandwidth.

Phaseless filtering can also be used to split the signal into subbands. The filtering is made phaseless by filtering twice. After the first filtering, the signal is reversed, filtered and reversed once again. The type of filter used depends on the preferences of the user. The use of phaseless filtering is important for identifying and monitoring evolution of AE sources. The fixed reference point enables the detection of trends in the signal. If phaseless filtering is not used then the identification and monitoring of evolving AE sources will be more difficult. This is because a phase lag will be caused by the filters and the lag will be different for different frequencies. For an evolving AE source which emits AE earlier and changes the frequency the phase lag could possibly delay the signal so that the change will not be detected.

2.3 Third step: Feature extraction

Over the years many research projects have been conducted with the aim of extracting useful information from AE signals. The extracted information is stored in n-dimensional data structures, known as features. Commonly used features for monitoring AE activity are number of AE hits and the signal's energy (Carlos & Vallen, 2005; Hellier, 2001). Conventional features extracted from AE hits include amplitude, duration, energy, number of peaks above certain threshold (ring-down count) and rise time (Carlos & Vallen, 2005). One of the advantages of extracting and using features is that they provide a huge data reduction compared with a full waveform acquisition, but there are several practical disadvantages. First, the fact that the same type of damage can emit AE signals with different amplitudes (Prosser et al., 1997) makes it difficult to set the threshold for hit detection and to interpret. Second, AE signals in composites suffer from high attenuation, which means that emissions close to the transducer are stronger and more likely to be detected than those generated further away. Third, the rugged frequency response of resonance AE transducers means that frequencies which are spaced only a few tens of kilohertz apart, will be magnified differently. The magnification can differ by several decibels. Finally, if only the AE features

are stored then the analysis is limited to these features, e.g. it is impossible to study different results using other threshold settings.

The procedure for extracting features from each subband segment, s_{sb}, is a two step procedure. In the first step the AE feature of interest is extracted from the segment and both the feature values and their locations within the segment are logged. In the second step, the segment is partitioned into K intervals and the features extracted within each interval are processed, e.g. occurrences counted or the maximum value picked. The user selects the number of intervals, K. The results from the processing are output in a feature vector ($K \times 1$), i.e. one vector for each feature. Depending on the processing in the second step, the first step can in some cases be omitted, e.g. when the energy in each interval or the maximum amplitude is computed. Figure 3 illustrates this procedure by showing how a a feature vector is generated when the maximum amplitude in each interval is used. Each subband segment is first rectified and partitioned into K intervals and then the maximum amplitude within the interval is found, i.e. a piecewise constant envelope is generated. The envelope is then down-sampled by a factor L/K, where L is the length of the subband segment. The resulting feature vector contains one sample from each interval of the envelope. The amplitude-filtering and down-sampling process extracts the amplitude of the strongest transient in each interval. Hence, the tracking capability is limited by this filtering. However, the filtering is performed in all the subbands, which consequently improves the tracking ability because the AE energy from different sources often resides in different subbands.

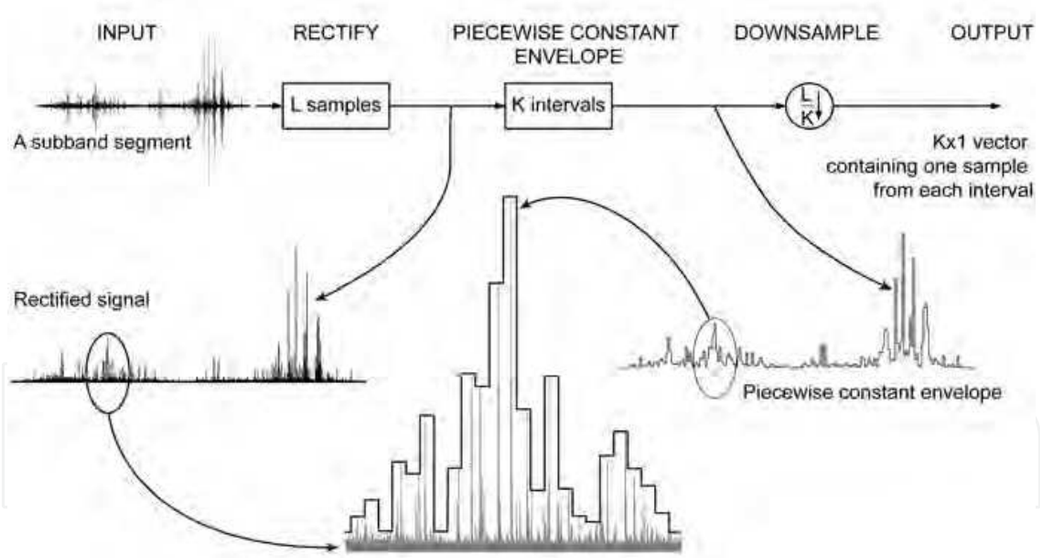

Fig. 3. For each subband segment, the new feature vector is computed by first rectifying the signal, then computing a piecewise constant envelope, and finally down-sampling the envelope.

2.4 Fourth step: Visualization

Visualization of measurement data is a powerful tool for detecting trends in complex data. In fact most AE analysis is done graphically using histograms or by plotting the feature of choice either as a function of time or as a function of another feature. The methodology

presented here is designed for detecting temporal trends in feature values and in the positions of emissions relative to a reference point in the reference signal. If one feature value is studied at a time, then the data becomes 3-dimensional. A convenient way for studying 3D data is by using a 3D surface. A 3D surface representation of the data is generated for each subband by appending each new feature vector to previous vectors from the same subband. The first step in Fig. 4 illustrates this procedure where the duration of one cycle (other parameters can be used) is on the x-axis, the segment number is on the y-axis and the feature value is on the z-axis.

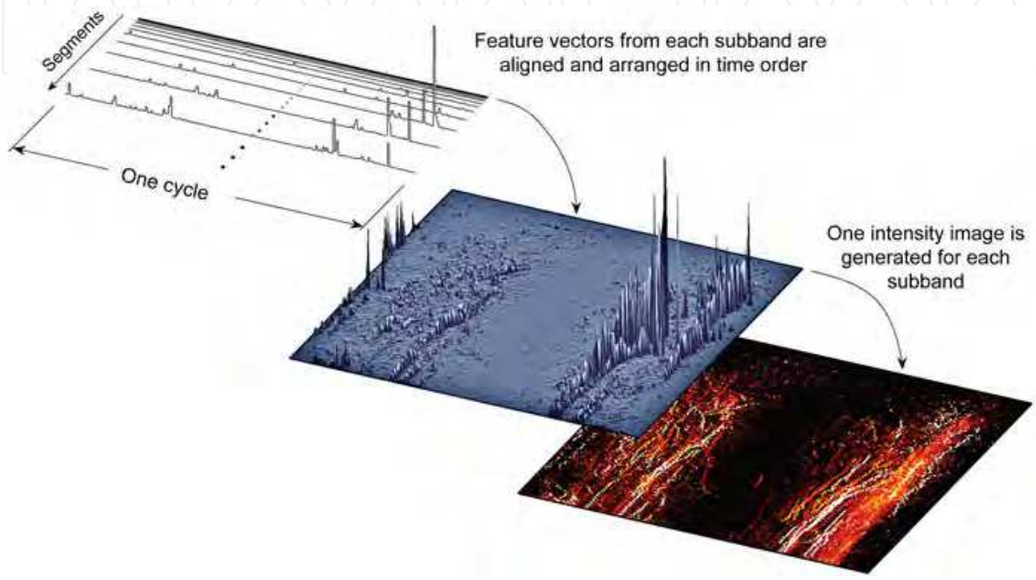

Fig. 4. For each subband, new feature vectors are appended to previous vectors and a 3D surface generated. The 3D surfaces can be converted into 2D intensity images for visualization and further processing.

Trends can be detected by visually inspecting the 3D surfaces, e.g. few trends can be detected from the 3D surface in Fig. 4. Any change in either the feature value or the relative position indicates an evolving AE source. AE from growing cracks will be emitted at different load/time and the corresponding feature value will shift on the x-axis. This type of a change will be seen as a curved ridge on the surface. Stationary AE sources will be represented by straight vertical ridges. Ascending and descending ridges need a special attention because the energy of the corresponding AE source may be shifting to another subband.

Another useful way to visualize the AE data is to use intensity images. Intensity images can be generated from 3D surfaces by transforming and colour coding the z-axis, i.e. the feature values. Logarithmic transformation, e.g. base-10, can be a good choice as it changes the dynamic range of the signal by enhancing low values, while compressing high values. Monochrome colour coding is often used for intensity images. By using monochrome coding the transformed feature values are represented in shades of one colour and the higher the value, the brighter the image pixel. A bright pixel shows the location of an AE source with a high feature value. The horizontal axis is the same as the x-axis in the 3D surfaces representation and shows the location of an source relatively to the phase of the reference signal. The segments are arranged on the vertical axis with numbers increasing from top to

bottom, i.e. the first segment is at the top of the image. The illustration in Fig. 4 shows the results of transforming a 3D surface into a 2D intensity image. The ridges on the surface appear as paths in the image and random AE sources appear as random points. Ascending and descending ridges can be identified by the changing pixel intensity in a path. The paths can be used to identify and monitor evolving AE sources and also to isolate the signal for further analysis. Advanced image processing can be applied to the images in order to enhance the images and to make the paths more prominent.

2.5 Summary

The methodology presented in this section was designed to facilitate trend detection and monitoring of evolving AE sources when the AE activity is high. Identification of evolving AE sources is performed by visual inspection of 3D surfaces or intensity images. These two visual representations are valuable for interpreting the AE behaviour and for gaining a deeper understanding of the active damage mechanisms. Trends can be relatively easy to identify from the intensity images but, the resolution and quality depend on the colour coding quantization and the coding range (the max/min values). Due to the limited number of quantized values a decreasing feature value may be detected later than when performing visual inspection of 3D surfaces. For a thorough inspection of a 3D surface, the user needs to have several tools at his disposal, such as rotate, zoom and section.

3. AE hit pattern feature

One of the fundamental elements of music is rhythm. Rhythm can be determined by the relation between note accents (attack) and the rests between notes (Olson, 1967). The term can be used to refer to either a repetitive pulse, or a beat, which is repeated throughout the music or a temporal pattern of pulses. The modelling and the interpretation of temporal patterns are of interest to people working in different disciplines. In the field of music information retrieval rhythm-based features have been extracted from audio and used to classify music styles (Dixon et al., 2003), e.g. blues, disco, polka, etc. In the field of computational neuroscience, patterns in spike trains are studied in order to understand the "language of the brain" (Rieke et al., 1997). For this reason, the author has formulated an AE feature to investigate whether patterns exist in AE signals and if they can be used to extract valuable information from the AE signal. This AE feature will now be introduced.

The first step in working with temporal patterns is to determine the pulses. The detection of pulses usually begins with the processing of the signal in order to make the detection more accurate. The resulting signal is called a detection function. An example of a detection function is one made using a model called a rhythm track (Sethares et al., 2005). The rhythm-track model is based on the assumption that the audio can be considered to be a random signal and the signal's energy increases significantly when a pulse occurs. The resulting rhythm track contains the locations of all the pulses. These pulses are known as AE hits when working with AE signals. An intuitive rhythm track is a vector, of the same length as the signal, containing ones where the AE hits start and zeros elsewhere.

Interpreting patterns in the rhythm-track is a challenging task because similar patterns can be generated differently. For example, closely spaced transients can be attributed to factors

such as rapid AE release, reflections, and simultaneous emissions from multiple sources. The results from an investigation into fusing AE features (Unnthorsson et al., 2005) provided an impetus to investigate the fusion of AE features with the rhythm track information. As a result, a methodology for fusing AE features, and for finding and locating patterns within the fused data representation, has been elaborated. The additional information provided by the waveform-based features comes at higher computational cost, but may help to distinguish and interpret rhythm track patterns which are generated differently, or at different locations.

The fused and coded AE features are collected in a vector, called a coding vector, where each hit is represented by a subvector. The length of the subvector, is the same for all hits but, depends on both the number and type of features used. In order to limit the number of patterns found in the coding vector the features are first processed and then their values are quantized to a relatively small set of integers. The quantization suggested here is to transform the processed features logarithmically ($\log_{10}$), then shift, scale, and round the results so that they are represented by integers ranging from 1 to $\mathrm{N}_{FEATURE}$, where $\mathrm{N}_{FEATURE}$ is an integer number chosen by the user.

The scaling operation requires the user to know the extreme values of the features. If the extreme values can only be approximated then the coded elements will be occasionally out of range. In order to solve this, hard limits can be used, i.e. if the values go out of range then they will be set to the allowable maximum. However, the limits do not have to be critical; if the coded elements are allowed to exceed the limit then relatively few new patterns will be added. Henceforth, the processing and quantization will be referred to as coding. The coding of each element depends on the corresponding feature.

Figure 5 illustrates how the coding vector is generated when two element subvectors are used. The elements of the subvectors, shown in the figure, are the coded maximum amplitude of the hit and the coded inter-spike interval (ISI) between the peaks of the current hit and the previous hit. The coding of the ISI is made by first logarithmically transforming ($\log_{10}$) the time between the peak amplitudes of successive hits, measured in milliseconds. The results are then quantized so that each ISI is represented by integer values ranging from 1 to N_{ISI}. The coding of the peak amplitudes is performed in a similar way. The amplitudes are logarithmically transformed ($\log_{10}$) and quantized to integer values between 1 and N_{AMP}.

The procedure for searching for hit patterns in the coding vector is illustrated in Fig. 6. The locations where a pattern, H_P, is observed are stored in an observations vector, O_P, where $P = 1, \ldots, N_P$ and N_P is the number of hit patterns. Each observation vector is of same length as the original AE signal and initially contains only zeros. The locations where a pattern, H_P, is observed within the AE signal are indicated by ones in the corresponding observation vector. The ones are placed where the patterns start.

3.1 Summary

This section introduced and formulated an AE feature which contains information about the timing between hits and a methodology for fusing it and coding with other AE features. The section also developed a procedure for searching for AE-hit patterns in the coded representation and formulating the search results. The experimental results from using this feature will be demonstrated in section 5.

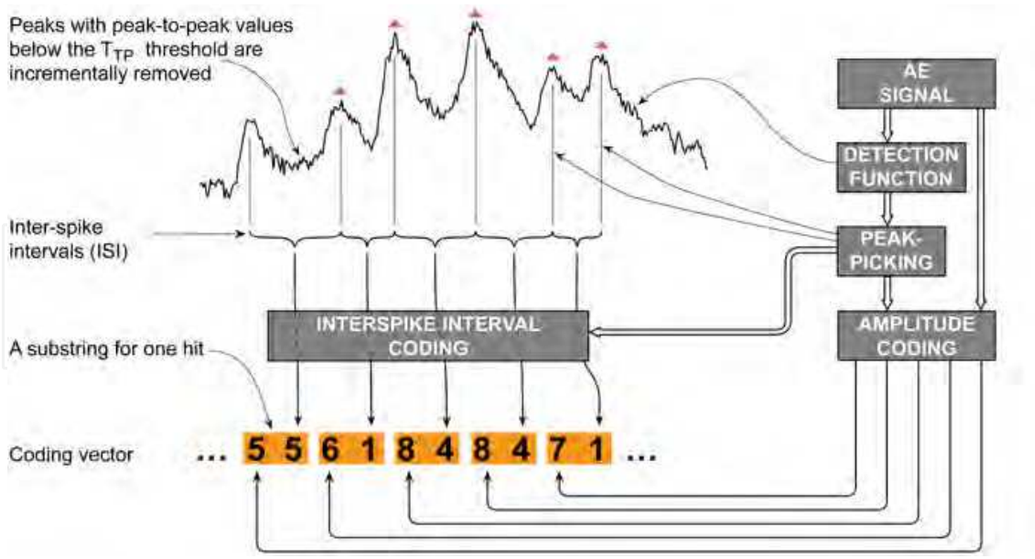

Fig. 5. The generation of the coding vector illustrated using two element subvectors for each hit. The two elements are coded maximum amplitude and coded ISI respectively.

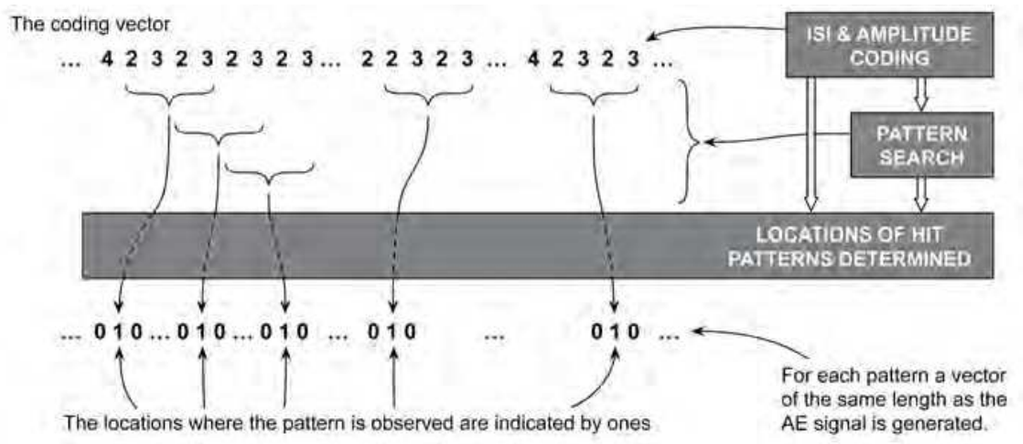

Fig. 6. The procedure for finding hit patterns in the coded representation.

4. Experimental setup

Experimental data is used for demonstrating both the methodology and the AE Hit pattern feature. An overview of the experimental setup is provided in this section. The section describes test specimen, the experimental procedure, and the equipment used. For detailed information about the experimental setup the reader is referred to author's PhD thesis (Unnthorsson, 2008).

4.1 The test specimen

The test specimen used in this study is an assembled prosthetic foot of the type Vari-Flex, made by Össur hf. The Vari-Flex consists of three CFRP composite components: a dual part heel and split-toe foot. In addition, a shock-absorbing crepe is glued under the forefoot. The

foot assembly is illustrated in Fig. 7. All components are curved with both varying thickness and width. Figure 7a depicts the varying thickness and Fig. 7b shows the split toe. A male pyramid, for fastening the foot to endoskeletal pylon components and the test machine, is bolted to the top of the foot component.

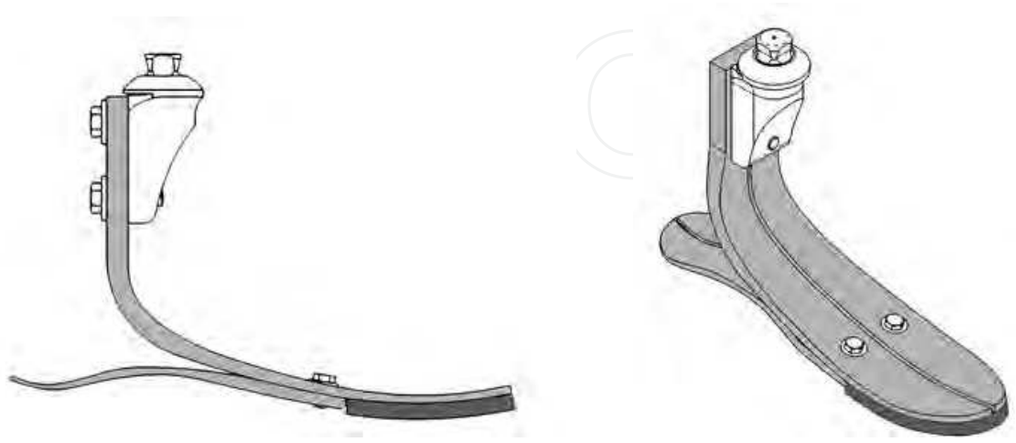

(a) A side view of the Vari-Flex. The diagram shows the varying thicknesses of the components.

(b) An isometric view of the Vari-Flex.

Fig. 7. The assembled Vari-Flex. The Vari-Flex is made up of two heel parts and one toe part.

The layer orientation and sequence are similar for all the components. The four outermost layers, on each side, are woven carbon/epoxy prepregs, laid at 45°. Between the outer layers unidirectional carbon/epoxy prepreg tapes are laid at 0°. The number of the unidirectional tapes differs between components and their lengths are varied in order to obtain varying stiffness, resulting in a tapered thickness. Around the holes, at the top of the foot, extra unidirectional carbon/epoxy prepreg tapes are laid at 90° for added strength.

4.2 Test setup & procedure

The fatigue tests were performed in an ISO 10328 Foot/Limb test machine run under PID closed loop control. In each test, a foot was placed in the test machine where two actuators were used to flex the foot using 90° phased sinusoidal loading. Figure 8 shows a schematic representation of the experimental setup. One actuator loaded the forefoot and the other loaded the heel. The actuator that flexed the forefoot was rotated 20° from the vertical and the one that flexed the heel was rotated $-15°$ from the vertical. Furthermore, the foot was rotated 7° out of the vertical plane defined by the movement of the actuators.

The maximum loading used was based on the stiffness category of the toe unit and the minimum loading was set to 50 N. In order to accelerate the tests the maximum loading was set 50% higher than is used for testing at Össur. In addition a 2° plastic wedge was placed between the heel and the toe components. The wedge is used by amputees in order to stiffen the foot. The increased load and the use of the wedge result in considerably shorter fatigue tests.

During one test, both the minimum and maximum loads were held constant, with allowable variation of $\pm 2\%$. The operating frequency was 1.0 Hz. It took the test machine approximately

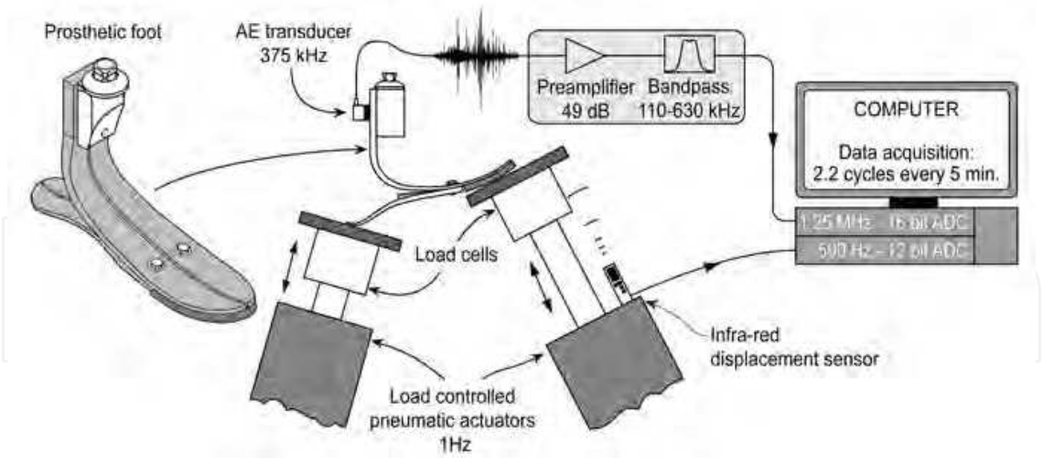

Fig. 8. Schematic representation of the experimental setup for both the AE and the position measurements.

1000–2000 cycles to reach the specified maximum and minimum load values. After this run-in period, the limits of the failure criterion were defined. The failure criterion is a heuristic criterion used in-house at Össur. It defines a failure when a 10% change in the displacement of either actuator, with respect to initial value, is observed. All fatigue tests were run until the failure criterion was met.

4.3 Data acquisition and processing

The additional parameter acquired simultaneously with the AE was the displacement of the forefoot actuator. Due to the geometry and structure of the Vari-Flex, the forefoot's actuator always meets the 10% displacement criterion before the heel's actuator. For this reason, only the position of the forefoot's actuator was measured. A L-Gage Q50A infra-red displacement sensor from Banner Engineering Corporation was used for measuring the position of the actuator. The sensor's location is illustrated in the lower left corner of Fig. 8. The analogue signal from the displacement sensor was digitally converted by a PCI-6024E 12 bit A/D converter (manufactured by National Instruments Corp.).

For acquiring the AE, the VS375-M AE transducer and the AEP3 preamplifier from Vallen Systeme GmbH were used. The transducer was located between the two bolts used to fasten the foot to the pyramid. This was the only part of the foot for where a full face contact with the transducer could be ensured. The transducer was held by a plastic c-clamp and a heavy duty high vacuum silicon grease from Wacker Chemie GmbH was used as coupling medium.

The gain of the preamplifier was set to 49 dB. The gain settings of the preamplifier are based on 28 VDC supply. The actual amplification, however, depends on the input voltage to the AEP3 preamplifier. With less than 28 V the saturation point is earlier and the gain goes down slightly. After consultation and discussion with the manufacturer 29.9 VDC was used. and powered using Velleman PS3003 – a linearly regulated laboratory power supply. A linear regulated power supply was recommended because switching power supplies may add unwanted noise. Table 1 lists the equipment along with the settings used.

AE acquisition	
VS375-M	An AE transducer with resonance at 375 kHz
AEP3	Preamplifier, 49 dB gain 110 kHz high pass filter (54 dB/octave) 630 kHz low pass filter (30 dB/octave)
DCPL1	Decoupling box
PS3003	Linearly regulated laboratory power supply 29.9 VDC
PCI-6250	16 bit A/D converter 1250 kHz sampling rate on one channel
Position measurements	
L-Gage Q50A	Infrared displacement sensor Fast response mode used
PCI-6024E	12 bit A/D converter 500 kHz sampling rate on one channel

Table 1. The measurement equipment used for acquiring AE and the position of the forefoot's actuator during fatigue testing.

The position of the forefoot's actuator and the AE signal were measured simultaneously at 500 Hz and 1.25 MHz sampling rates respectively. In order synchronize the two A/D converters their Real-Time System Integration (RTSI) buses were connected. The data was acquired automatically, for 2.2 seconds every 5 minutes. After the data acquisition, the data was trimmed so that it represented exactly one fatigue cycle, starting at the lowest position of the forefoot's actuator. The data was also high-pass filtered in order to remove DC and other low frequency disturbances. A fifth-order elliptic filter with 1 dB passband ripple and corner frequency of 80 kHz was used. The stopband attenuation was set to 30 dB at 50 kHz. No attempts were made in order to correct the acquired signal, i.e. remove the amplification made by the preamplifier and the transducer.

4.4 Summary

This section presented the test specimen and the test equipment used. An accelerated fatigue testing procedure was also presented. Frequently the damage mechanics change when the stress level changes, however, preparatory tests showed that the damage mechanisms leading to final failure were the same as observed under normal fatigue testing conditions.

5. Experimental results

Experimental data was acquired from fatigue testing of 75 nominally identical samples of the prosthetic foot. This section presents a case study of one foot and is split into three subsections. In the first subsection the evolution of few AE features throughout the fatigue life of the foot are studied and compared against their average evolution. The second and the third subsections present an in-depth analysis of the experimental data using conventional AE features and AE Hit patterns respectively. Both subsections show how the results provided by methodology can be used to facilitate early damage diagnosis and failure.

5.1 Evolution of AE features

The evolution of few AE features throughout the fatigue life of one prosthetic foot will now be studied. Each feature is overlaid onto its corresponding mean and standard deviation. Both are computed by from the evolution curves of all the other feet. The gray area in Fig. 9 and Fig. 11 represents all values which lie within one standard deviation from the mean. The position measurements of the forefoot's actuator are converted to cycle time and used as a reference signal for segmenting. The segments start at the lowest position of the actuator, or at 0° phase angle, and end when the actuator returns back to this position. Because the actuator moves at a constant angular velocity the segments are all of equal length. The features are extracted from the whole segment and without subband filtering or, in the terms of the methodology presented in 2, the features are extracted by using one interval ($K = 1$) and the signal's full bandwidth ($N = 1$).

Based on the results of visual and acoustic inspection performed by the author, i.e. watching and listening, during the cyclic testing of the foot, the temporal behaviour of the AE features are interpreted. Detection and determination of AE hits is made using the methodology presented in (Unnthorsson et al., 2008a) and (Unnthorsson, 2008). The STFT detection function is used, with segment size of $k = 128$ samples and $d = 120$ sample overlapping. The hits are located by setting the trough-to-peak threshold (T_{tp}) at 304 dB V-s and determined by setting the determination threshold (T_{AE}) at 3 mV.

Shortly after the cyclic test was initiated, or after 6k cycles, small splinters started to form on both sides of the split-toe foot. During the next 4.2k cycles the splinters grew larger and rubbed against the sides. As can be observed in Fig. 9, this resulted in a very steep increase in the AE energy, but only a slight increase in the number of AE hits. Two spikes can be observed in the AE energy when 12.3k and 13.2k cycles have elapsed. At this time a medium-sized splinter formed on the right side of the split-toe foot. The two measurements corresponding to the spikes in AE energy were taken at points when the splinters were growing. This means that the readings are composed of AE from both rubbing and damage growth. Thus, spikes are observed rather than a permanent increase. The reader is reminded that measurements are made at 5-minute intervals, or every 300 cycles; hence, the probability of recording AE from damage growth is low.

In the interval between cycles 15k to 18.6k cycles, a large splinter on the right side of the split-toe foot had formed. The splinter, depicted in Fig. 10a, caused both the upward and downward bending stiffnesses to drop. As a consequence, the displacement of the forefoot's actuator increased abruptly. The abrupt displacement increase will be referred to as step (or event) A. The formation of the splinter was accompanied by an increase in the AE energy and an abrupt jump in the AE hit count.

Within a few cycles after the formation of the splinter, or when 21.6k fatigue cycles had been applied, the outer woven layers on the left side delaminated from the unidirectional layers. The delamination crack initiated from the splinter crack and grew for undetermined number of cycles. The number of cycles is undetermined because it was not possible to establish if and when the crack growth stopped using visual inspection. In each cycle, when the crack opened an audible AE was produced. Due to this and also because the crack grew over time, the AE energy increases. From 21.6k to 28.5k cycles the AE energy increased at a relatively

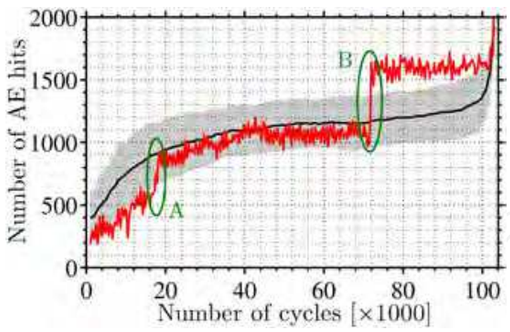

(a) The evolution of the AE hit count.

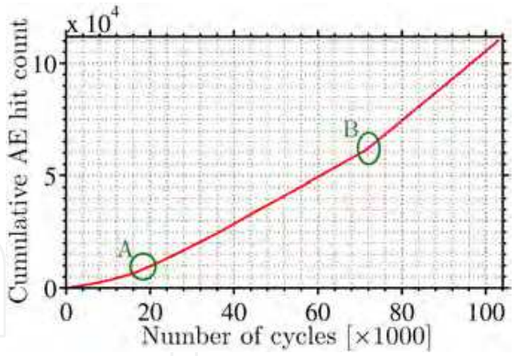

(b) The evolution of the cumulative AE hit count.

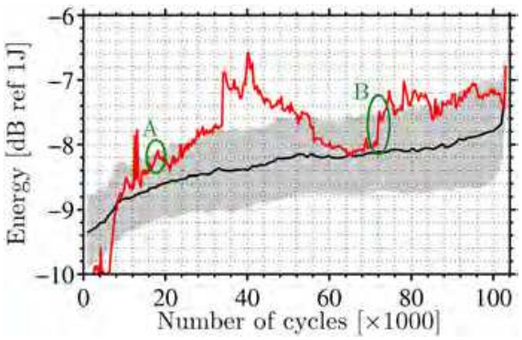

(c) The evolution of the energy

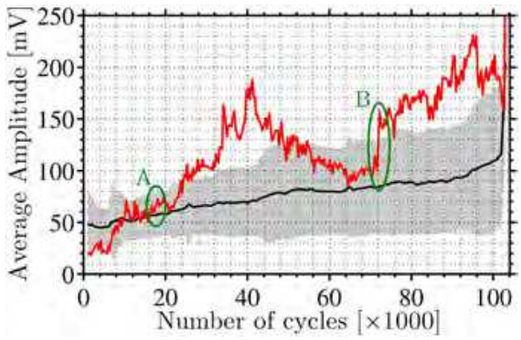

(d) The evolution of the average amplitude

Fig. 9. The evolution of selected AE features throughout one fatigue test. The grey area for each feature represents all values which lie within one standard deviation from the mean (black curve). The mean is computed by averaging the evolution curves from all other feet.

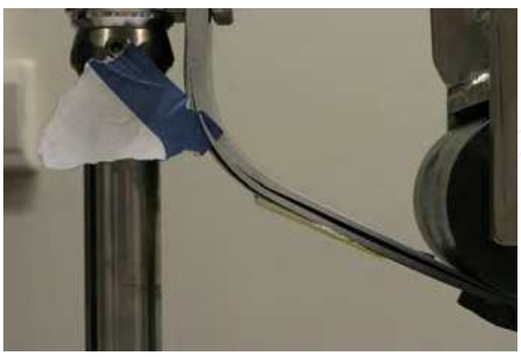

(a) Right side of the split-toe foot under static loading.

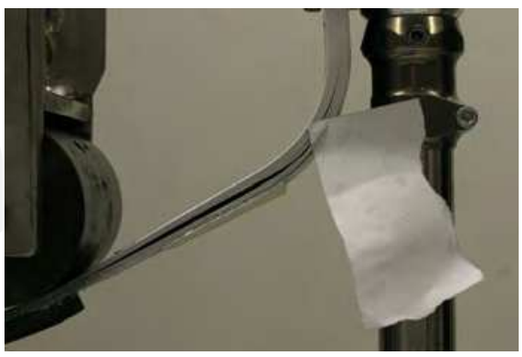

(b) Left side of the split-toe foot under static loading.

Fig. 10. The left and right sides of the split-toe foot after cyclic testing.

steady high rate, but then it became constant. At 28.5k cycles a medium-sized splinter formed on the left side. The splinter, shown in Fig. 10b, did not affect the bending stiffnesses and was not detectable in the evolution of any of the AE features. At 33.9k cycles there was an abrupt

jump in the AE energy and over the next 4.1k cycles the energy fell back by 50% of the jump. Shortly after that, or at 40.2k cycles, another abrupt jump in the AE energy occured. From this point the energy started to decline, initially at a high rate, but the rate decreased temporarily at 41.7k cycles, and then resumed at 55.2k cycles for 900 cycles. After this, the energy reduced at a low rate until the reduction ceased, at 64.8k cycles The two abrupt jumps in the energy, at 33.9k and 40.2k cycles, were not accompanied by any changes in the bending stiffnesses. Subtle changes, however, could be detected in the slope of the AE hit count, and duration at 40.2k cycles.

At 72k cycles, the left half of the split-toe foot delaminated. This resulted in a drop in the bending stiffnesses. The corresponding abrupt displacement increase will be referred to as event B. Both events are shown in Fig. 9 and Fig. 11. Abrupt jumps in the AE energy and AE hit count were also observed.

The cumulative AE hit count, presented in Fig. 9b, is a commonly used parameter for the study of acoustic emission. Although the cumulative sum contains the same information as the AE hit counts, the information provided by subtle slope changes, small jumps, and fluctuations is harder to detect. One can observe from the figure that the curve can be divided into three segments, each with a different slope. The slope changes occur at events A and B. However, the AE hit count, shown in Fig. 9a, is the slope of the curve in Fig. 9b at every measurement. The AE hit count is absolute in that it does not depend on prior values, but each value of the cumulative curve depends on all prior values. This means that missing or late measurements do not affect the results when monitoring the AE hit count, but the slope of the cumulative curve is a function of the frequency of the measurements, i.e. different curves are obtained by summing up the AE hit counts from measurements made at different or irregular intervals. Hence, the cumulative AE hit count works best when the interval between the measurements can be fixed.

The evolution of the average amplitude, depicted in Fig. 9d, is strongly correlated with the AE energy on a decibel scale, shown in Fig. 9d. The Pearson and Spearman correlation coefficients for the two curves are 0.88 and 0.92 respectively.

The AE hit pattern feature used is computed by first determining the time from a trough to a peak (and also from a peak to a trough) for each AE hit, then coding the results and then counting the occurrences of all patterns found in the coded representation. A trough-to-peak interval is a variant of the Inter-spike Interval (ISI). It can also be recognized to include variants of two commonly used AE hit-based features, namely the rise time and the fall time.

The methodology described in Sect. 2 is used to count the pattern occurrences. The AE hits are located using the procedure described above, but no determination is performed, i.e. the determination threshold (T_{AE}) is set to 0 mV. The trough-to-peak intervals, in microsecond, are quantized by using a natural logarithm and rounding the result to the nearest integer.

Figure 11 shows the evolution of the total number of observations for four selected trough-to-peak patterns of length 2. These patterns contain the coded values of the fall time of one hit and the rise time of the next adjacent hit. The evolution curves of the trough-to-peak patterns have a slope change at around 60% of the lifetime. The slope then remains constant until failure. This slope change is not present in the evolution curves for the other AE features. This suggests that these trough-to-peak pattern features are capturing important information

from the AE signal, e.g. the slope change may be caused by the formation of a damage which grows until failure. Intuitively, the salient slope change can be used to provide an early warning about the health of the composite.

In (Unnthorsson et al., 2008b) the trough-to-peak patterns were the only features studied which probability distributions at 50% and 95% of the lifetime could be reasonably well separated using a Bayes optimal decision boundary. The Bayes optimal decision thresholds are shown in Fig. 11. Patterns made using different coding, length, features, or a combination of features, can possibly be used to obtain more information. The additional information can be combined into a feature vector which can be used as an input into classifier system for more accurate warnings.

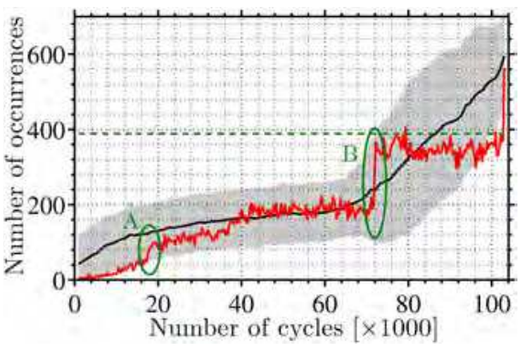

(a) The evolution of the number of occurrences of trough-to-peak pattern no. 87.

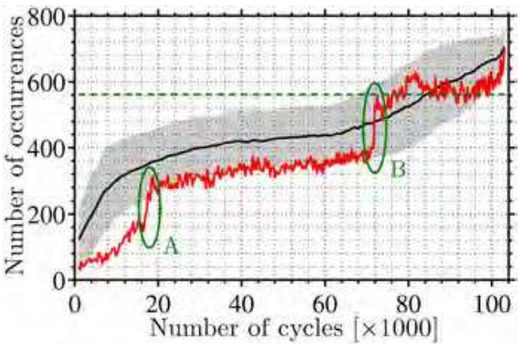

(b) The evolution of the number of occurrences of trough-to-peak pattern no. 94.

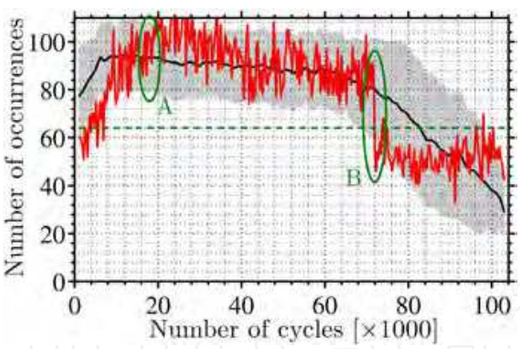

(c) The evolution of the number of occurrences of trough-to-peak pattern no. 95.

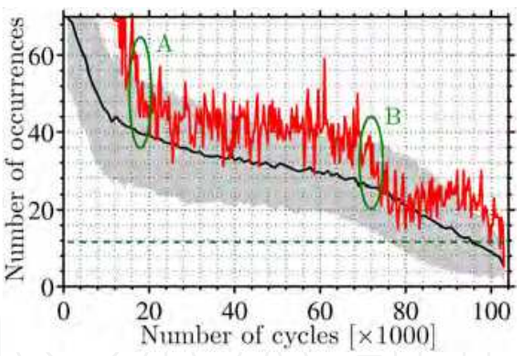

(d) The evolution of the number of occurrences of trough-to-peak pattern no. 102.

Fig. 11. The evolution of the number of occurrences for four trough-to-peak (ISI) patterns computed from the AE segments. The grey area for each pattern represents all values which lie within one standard deviation from the mean (black curve). The mean is computed by averaging the evolution curves from all other feet.

5.2 AE feature tracking

The results presented above were obtained by using one interval ($K = 1$) and full bandwidth ($N = 1$). In this subsection each subband segment is divided into $K = 200$ equally-sized

intervals and phaseless filtering is used to bandpass filter the AE signal into $N = 19$ subbands, each with 33 kHz bandwidth. By dividing the segments into shorter intervals, the dimension of time within a segment is added to the analysis. Furthermore, by bandpass filtering the signal and studying each subband separately the results are divided into N different subresults, one for each subband. For visualizing the results 2D intensity images will be used.

Figure 12 shows the resulting intensity image for the 133–166 kHz subband using the maximum amplitude of the rectified signal in each interval to generate the feature vector. The procedure is explained in Fig. 3. Also depicted in the figure is the evolution of the AE energy and the AE hit count. The AE energy and the hit count are computed the same way as was done in last subsection, i.e. by setting $K = 1$ (one interval) and $N = 1$ (full bandwidth).

Figure 13 shows four more intensity images corresponding to the 266–300 kHz, 366–400 kHz, 466–500 kHz and 566–600 kHz subbands. By comparing the evolution of the AE energy and the AE hit count in Fig. 12 against the intensity images depicted in Fig. 12 and Fig. 13, one can see that the intensity images facilitate a better understanding of the changes which occur in the material than the evolution of the AE features in last subsection.

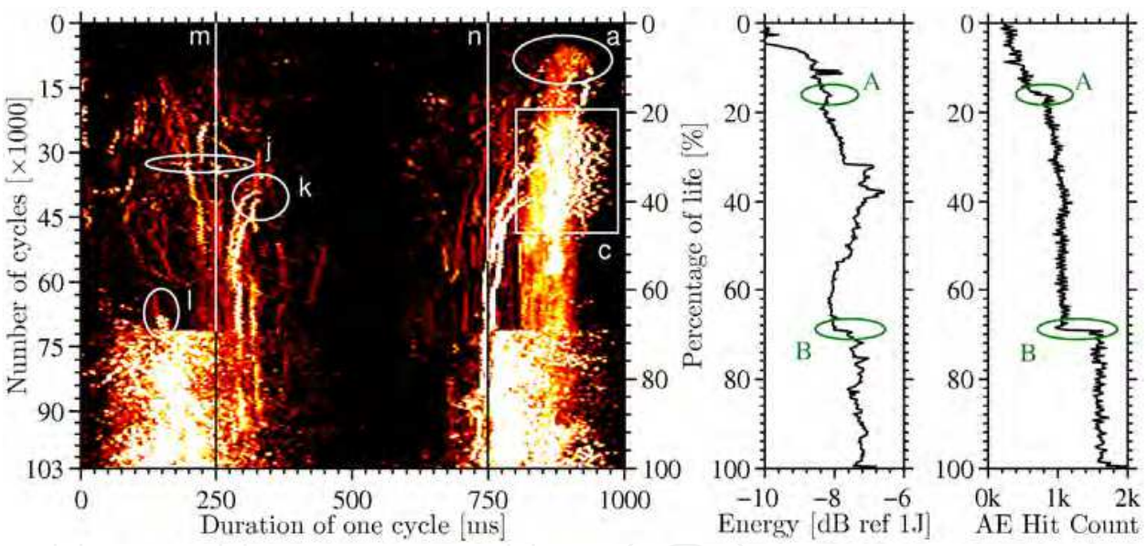

Fig. 12. On the left is the resulting intensity image for the 133–166 kHz subband. Each value in the image is the maximum amplitude in the corresponding interval. On the right is the evolution of the total AE energy and AE hit count from each segment (computed using the signal's full bandwidth).

The steep increase in the AE energy early in the fatigue test is attributed to formation of small splinters on the side of the split-toe foot. In each fatigue cycle these splinters rub against the toe-foot component and occasionally grow. The AE from these splinters is presented as a growing cluster in the upper left corner of the intensity image in Fig. 12. The cluster is circled and labelled a. At 12.3k and 13.2k cycles two spikes are observed in the evolution of the AE energy. These spikes are due to the formation of a medium-sized splinter on the right side of the split-toe foot. Although the AE energy only shows two spikes, one can see, from the intensity images, two new paths initiate at this time from within the cluster labelled a (Fig. 12). The paths are circled and labelled b (Fig. 13d).

A large splinter on the left side of the split-toe foot forms during the period from 15k to 18.6k cycles. The splinter causes a drop in both bending stiffnesses and can be detected as a subtle change in the evolution of the AE energy, but as an abrupt jump in the AE hit count (labelled A in Fig. 12. In the intensity images, this event can be detected by the formation of new paths and a sudden change in the left path of the two circled and labelled b (Fig. 13d). The left path changes its course, shifts to the left and disappears.

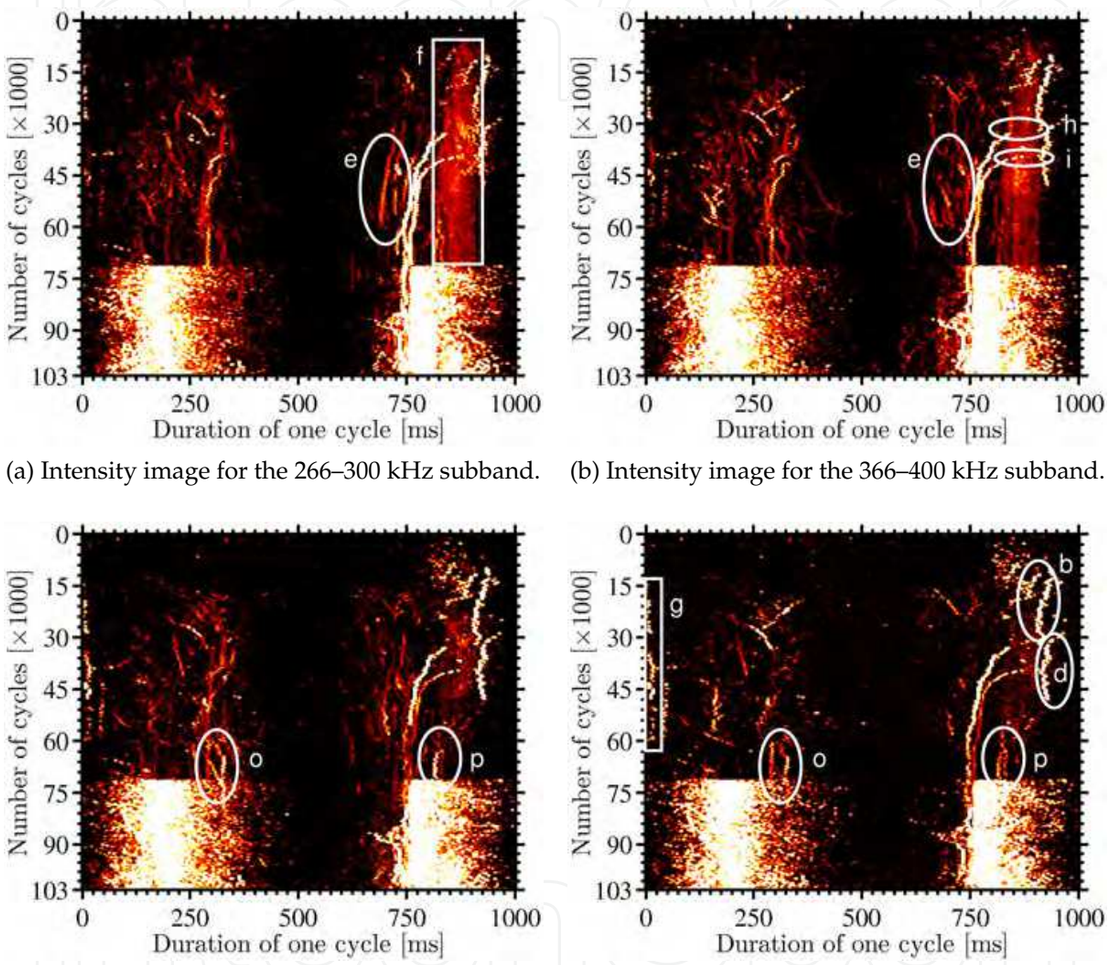

(a) Intensity image for the 266–300 kHz subband.

(b) Intensity image for the 366–400 kHz subband.

(c) Intensity image for the 466–500 kHz subband.

(d) Intensity image for the 566–600 kHz subband.

Fig. 13. The resulting intensity images for four selected subbands. The brightness of each pixel is based on the amplitude in the corresponding interval.

Within a few hundred cycles after the formation of the splinter, the woven layers at the left bottom of the split-toe foot delaminate from the unidirectional layers. The delamination crack opens every time that the heel's actuator is nearly fully loaded and an audible AE is generated. The crack grows and the AE energy increases at a steady high rate. The AE from the delamination crack resides in the lower frequency bands and can be observed in the boxed area labelled c (Fig. 12). In the 133–166 kHz subband, the AE from the delamination crack

masks out other AE. However, the AE is bandlimited; hence, different frequency bands can be used to monitor some of the masked-out damages, e.g. the circled paths labelled b and d (Fig. 13d).

At 28.5k cycles a medium-sized splinter forms on the left side of the split-toe foot. The formation cannot be detected from the the evolution of the AE energy, AE hit count nor the bending stiffnesses. The AE emitted from the splinter is masked out in the 133–166 kHz subband, but can be detected and monitored in intensity images for the higher frequency bands. The corresponding evolution path is circled and labelled d in Fig. 13d.

By studying different subbands, one can in some cases detect and distinguish between damages that emit bandlimited AE signals at the same time, but are evolving in different directions, as can be seen by comparing the circled paths labelled e in Fig. 13b and Fig. 13c. Most of the energy from the frictional AE caused by the rubbing of the splinters is located in the lower frequencies. The boxed region labelled f (Fig. 13a) shows where the frictional AE is located within the fatigue cycles. In addition to the frictional AE, the splinters also, for a limited time, produce strong AE at the end of their push-out movement (the circled paths labelled b and d in Fig. 13d) and also when they snap back in (the boxed area labelled g in Fig. 13d).

The two abrupt jumps in the AE energy and amplitude at 33.9k and 40.2k cycles are accompanied only by subtle changes in the slope of the other AE features, but no changes in the bending stiffnesses. The intensity images, however, show the initiation of two paths originating from within the area where the frictional AE from the splinters is located. The area of initiations are circled and labelled h and i in Fig. 13b.

In the first half of the segment in which the first path starts (labelled h in Fig. 13b), a high amplitude AE can be observed in the intensity image for the 133–166 kHz subband (Fig. 12). This portion is circled and labelled j. Furthermore, two evolving high amplitude paths end in this portion. Simultaneously with the initiation of the second path, labelled i (Fig. 13b), another high amplitude AE path initiates in the first half of the loading cycle. The path can be seen in all subbands. The beginning of the path is circled and labelled k in Fig. 12. The two paths, labelled h and i (Fig. 13b), evolve asymptotically towards a line close to and parallel to the 750 ms line, labelled n in Fig. 12. Initially the paths evolve at a high rate but as they approach the line the rate decreases. The vertical asymptote line is located where the tensional, compressional and shear stresses change their signs. This location in the fatigue cycle acts as an attractor for most evolving AE sources in the left half of the intensity images, i.e. during the downward movement of the forefoot's actuator. Conversely, during the upward movement of the actuator, the so-called attractor is around 250 ms, shown by a line labelled m in Fig. 12. As can be observed in the figure, the attractor is offset to the right. This is because the the loading is not symmetrical around the 500 ms.

The left half of the split-toe foot delaminates at 72k cycles. This event (labelled B in Fig. 12) can be observed in the evolution of all AE features and also in the downward bending stiffness. After the delamination, a high amplitude AE is generated in a large portion of each cycle and in all subbands. During the 12k cycles leading up to the delamination the AE activity, as indicated by the evolution of the AE features in Fig. 9, remains at a relatively steady

level. However, the intensity images show few changes which can be interpreted as warnings. First, several new high-amplitude paths start during this period. These paths are circled and labelled l, o and p in Figs. 12, 13c and 13d. Second, during this period one can observe that the path which began in the circled area labelled h moves one step closer to the 750 ms line.

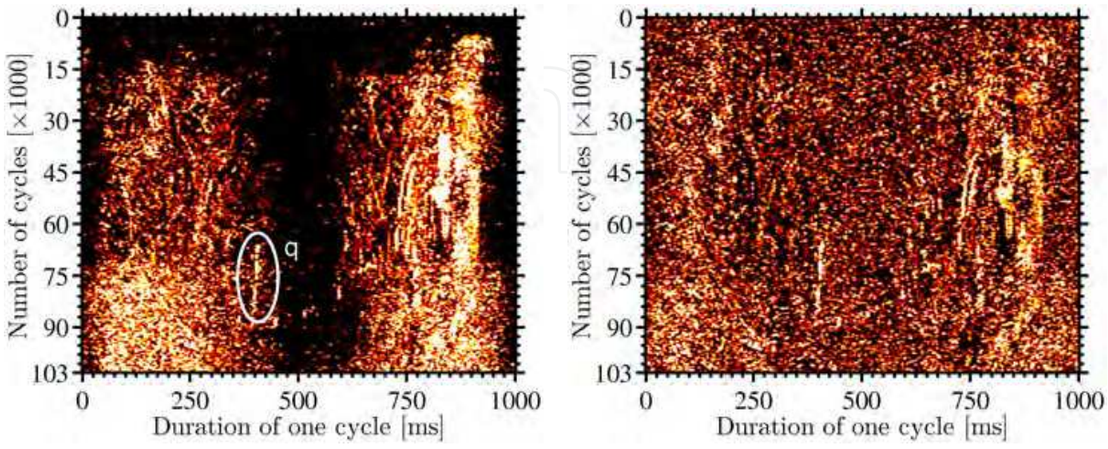

(a) Intensity image computed using the ring-down counts of the hit with the maximum amplitude in each interval.

(b) Intensity image computed using the duration of the hit with the maximum amplitude in each interval.

Fig. 14. Two intensity images, for the 133–166 kHz subband, made using threshold-based AE features. The brightness of each pixel is based on the value of the AE feature in the corresponding interval.

The AE energy feature produces nearly identical results to those presented here. Figure 14a and Fig.14b show results computed using the ring-down counts and the duration of the hit with the maximum amplitude in each interval respectively. In order to compute the features, the determination threshold, T_{AE}, is set to 3 mV. These images do not have as well defined paths as the images presented above, but different features can reveal new patterns (e.g. the circled path labelled q in Fig. 14a). The main challenge in using this approach for threshold-based features is the task of adjusting for each subband the trough-to-peak threshold, T_{tp}, used for locating hits from the detection function, and the determination threshold, T_{AE}, used both for determining hits and for extracting the threshold-based features.

5.3 AE pattern tracking

The results presented above were obtained using the maximum amplitude in an interval. Also demonstrated were results from using both the ring down count and the duration of the hit with the largest amplitude in an interval. Here the results of using AE-hit patterns will be presented. The segmentation and subband filtering as before, i.e. $K = 200$ and $N = 19$.

The algorithm for detecting hits is adjusted for each subband so that the average number of detected hits in the first 5 measurements is around 10.000. In other words, the average pulse duration in each subband is 0.1 ms. By using these settings small pulsations in the AE signal's amplitude are detected as hits but, the hit determination is the same as before, i.e. $T_{AE} = 3$ mV.

Two different coding representations are studied: one using only ISI information, and another using both ISI and the peak amplitude of the hits. The values of N_{ISI} and N_{AMP} are both set to 10 when computing the feature vectors. The resulting feature vector for each pattern contains the total number of observations in each interval. In order to fight the curse of dimensionality only two pattern lengths are used for both coding representations: $L = 2$ and $L = 4$.

5.3.1 ISI coding

Approximately 60 patterns are found in each subband when using ISI coding. However, only a handful of them produce intensity images with detectable paths. Figure 15 shows an example of two intensity images which have no detectable paths.

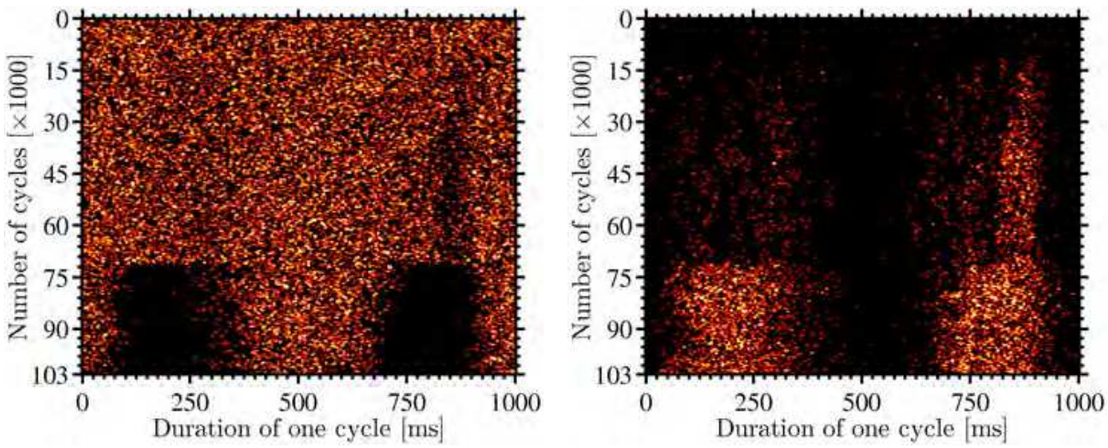

(a) An intensity image for an ISI pattern which does not show any paths.

(b) An intensity image for an ISI pattern which does not show any paths.

Fig. 15. Two intensity images which have no detectable paths. The brightness of each pixel is based on how often a pattern is observed in the corresponding interval.

Figure 16 shows intensity images for four handpicked patterns. As one can observe, the circled paths labelled 1, 2, 3 and 6 in the figure are the same paths as those depicted in Fig. 12 and Fig. 13. However, further comparison of the images, in these three figures, shows that only small portions of the circled paths labelled 4 and 5 in Fig. 16 can be detected in the other two figures. Consequently, by using AE patterns based on the ISI, more defined and more visually detectable paths can be detected. These paths can be used to locate AE sources for tracking and for detailed analysis of their AE signals.

Figures 16b and 16c show that different patterns may be used to monitor the same AE source. This is because the ISI, as used here, is the based on the time between the small pulsations in the AE amplitude and the AE emitted from a source may contain several patterns.

The intensity images for some patterns do not have any prominent paths, but instead clusters. An example of such an image is shown in Fig. 16d. The high values in this image are clustered where the frictional AE is emitted, indicating that some patterns may be used to monitor frictional AE.

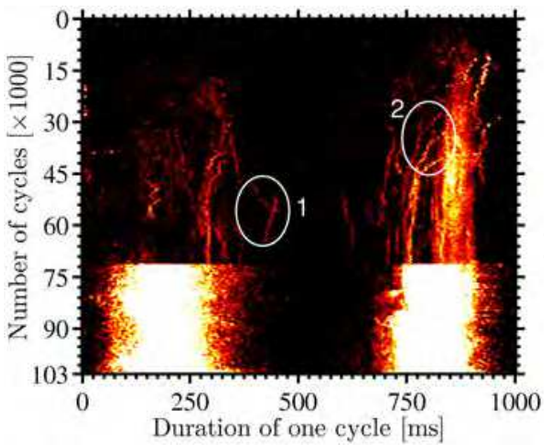

(a) Intensity image for a pattern in the 333–366 kHz subband.

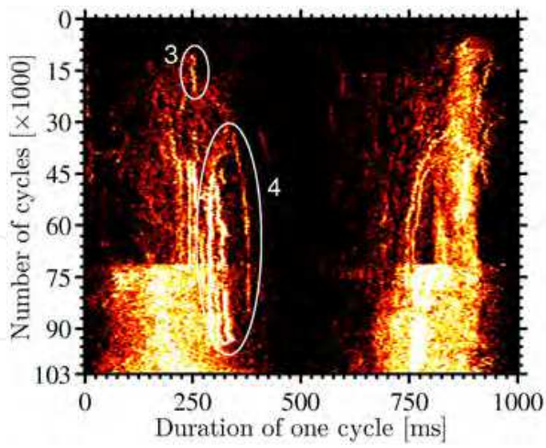

(b) Intensity image for a pattern in the 133–166 kHz subband.

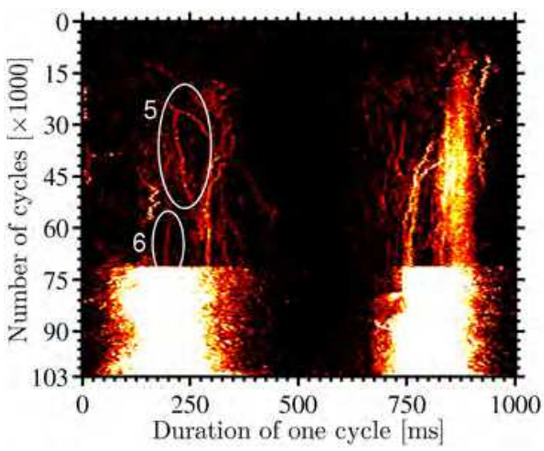

(c) Intensity image for a pattern in the 366–400 kHz subband.

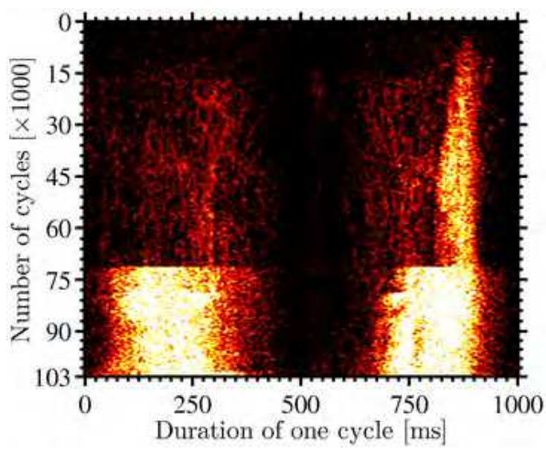

(d) Intensity image for a pattern in the 366–400 kHz subband.

Fig. 16. Intensity images corresponding to four selected ISI patterns. The brightness of each pixel is based on how often a pattern is observed in the corresponding interval.

5.3.2 ISI/peak amplitude coding

By combining the ISI coding with the peak amplitude, the total number of patterns increases up to approximately 600 patterns for each subband. The increase is a function of the number of quantization levels used for the amplitude,N_{AMP}.

Figure 17 shows intensity images corresponding to four handpicked patterns. The circled paths labelled I, III and IV can also be detected in the images obtained using only ISI coding (see Fig. 16b). However, these paths are more prominent in Fig. 17. This is because the addition of the peak amplitude works like a filter. The observations of patterns with certain ISI coding are divided between patterns with the same ISI coding, but different amplitude coding. As a result, the number of AE patterns is higher. This filtering helps with detecting patterns which would otherwise pass undetected, e.g. the circled paths labelled II in Fig. 17b.

By visually inspecting the intensity images for different patterns and extracting prominent paths, e.g. those circled in Fig. 17, a composite image can be made by piecing together the individual paths. Figure 18 shows a composite image, made by picking out, overlaying and enhancing paths extracted from 32 handpicked intensity images. The images are from all subbands. On the right side the composite image is the evolution of the AE energy in each segment.

A comparison of the intensity images in Fig. 16 with the intensity image in Fig. 18 reveals that the addition of the peak amplitude makes it possible to track the evolution of several AE sources after the left half of the split-toe foot delaminates at 72k cycles. The tracking improvement can also be observed by comparing the 750-1000 ms region of the images (where the frictional AE due to the rubbing of the splinters is located). In this region of the fatigue cycle, the initiation of 3 paths can be observed (indicated by arrows). Furthermore, the first path, which starts at event A, can now be tracked until shortly before the delamination of the left half. Based on these results, it can be deduced that the splinters initiate damages which grow until delamination occurs.

5.4 Discussion and summary

In this section the methodology was demonstrated and used for two different purposes. One is for general health monitoring where the evolution of a feature, extracted from each segment, is monitored in order to detect changes and issuing timely warning signs. The other is for detailed health monitoring where individual AE sources are identified, their evolution monitored and their nature determined.

The results show that none of the AE features studied here is suitable for general health monitoring. None of the features could be used to give timely warnings about the delamination which occurs at step B when the method of extracting one AE feature from each segment and studying its evolution is used. The abrupt jumps in the AE energy (and the average amplitude) at 33.9k and 40.2k cycles may perhaps be considered as early warning signs. However, because the AE energy decreases rapidly after the jumps and no significant changes are observed in the evolution of the other AE features, nor in the bending stiffness, nor from the visual tests, the potential warning signs cannot be interpreted or verified. Although these results are discouraging, there are also positive results. The average evolution curve of the four selected hit patterns has a slope change at around 70% of the lifetime. This is different from the other features studied and indicates that pattern features are able to capture important information from the AE signal.

The results show that the methodology is a valuable tool for detailed health monitoring. By using a conventional AE feature such as the maximum amplitude in an interval, valuable information about the location and the evolution of multiple AE sources was obtained. The results obtained using other hit-based features indicate that they are not good for this task. The sources are identified and monitored using the paths in the resulting intensity images. The nature of sources can also be determined by studying the paths (evolving or stationary source) or clusters (rubbing) in the images. Furthermore, by bandpass filtering the AE signal and studying each subband separately, band-limited AE sources can be identified and monitored. These sources may otherwise pass unnoticed.

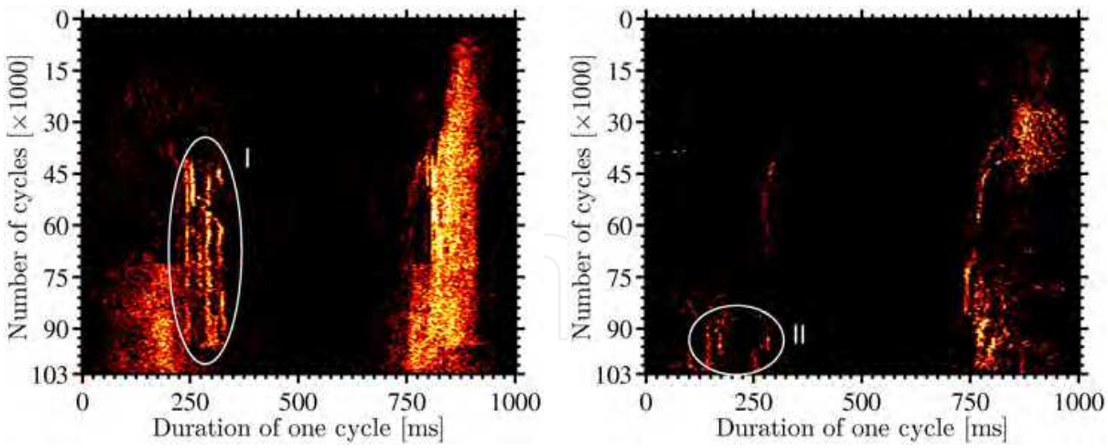

(a) Intensity image for a pattern in the 100–133 kHz subband.

(b) Intensity image for a pattern in the 100–133 kHz subband.

(c) Intensity image for a pattern in the 133–166 kHz subband.

(d) Intensity image for a pattern in the 133–166 kHz subband.

Fig. 17. Intensity images corresponding to four handpicked patterns. The brightness of each pixel is based on how often a pattern is observed in the corresponding interval.

From the resulting intensity images, the initiation of two AE sources was identified and tracked until delamination of the foot. Visual inspection of the intensity images revealed that the corresponding paths initiated where the AE from the splinters was located. This suggested that the corresponding damages were caused by the splinters. Hence, the paths can be used to significantly improve our understanding of the changes occurring in the material, and lead to more focused analysis of the AE signal. The analysis becomes more focused and detailed because it is possible to locate the AE from one particular AE source in the subband of interest. This means that the detection of paths is important for all further analysis and interpretation of the AE signal. The important task is therefore to find all existing patterns.

The results show that the AE patterns made from inter-spike intervals (ISI) can be used to track the locations of AE sources. The paths obtained using the patterns are nearly the same

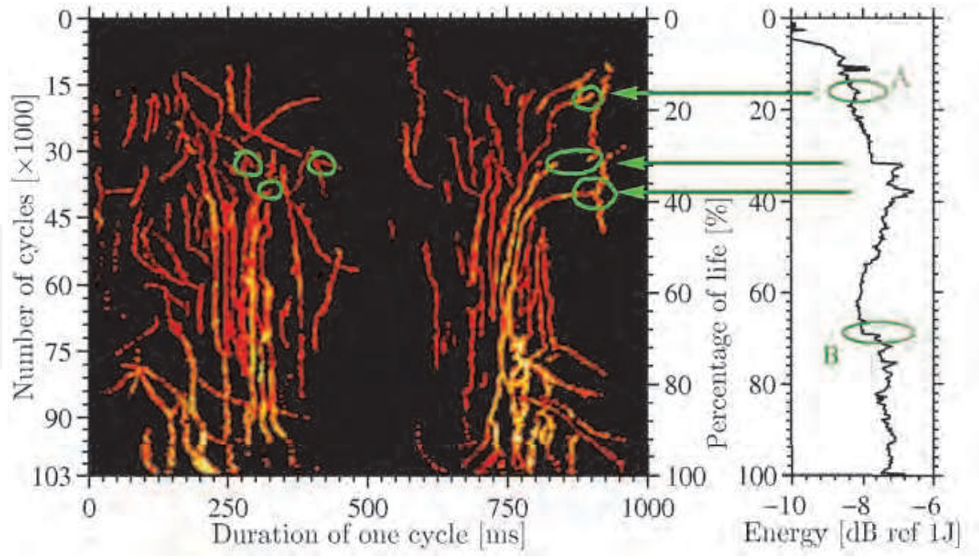

Fig. 18. On the left is a composite image made by overlaying and enhancing the results from 32 patterns. On the right is the evolution of the AE energy.

as the those obtained using the AE energy. A significant improvement was accomplished by combining the ISI information with the peak amplitude of each hit. This is because the addition of the amplitude acts like a filter on the results obtained using ISI patterns. Hence, by adding the peak amplitude it is possible to track evolving sources when they are buried in AE from delamination or rubbing. It can also be used to do the opposite: to filter out and monitor the evolution of a rubbing AE.

6. Conclusion and future research

This chapter presented a methodology for identifying and monitoring evolving AE sources and demonstrated it using experimental data acquired during fatigue testing of assembled CFRP prosthetic feet. By using this methodology, both frictional AE and AE from evolving damage growth could be identified, located and tracked. Furthermore, because AE from specific AE sources can be identified and isolated, further analysis of the AE can be made more effective. The methodology can be used to study changes, or artifacts, in AE or other signals using either periodic or aperiodic reference signals. Examples of signals which can be studied include AE from relays and valves (aperiodic), vibrational data, charging/discharging of batteries, etc.

The chapter also presented a procedure for extracting/generating an AE hit pattern feature. The AE hit pattern feature is a technique for: a) fusing the features extracted from AE hits, b) combining the fused data, and c) finding and locating patterns which appear within the fused data representation. The favourable results show that the AE hit pattern features can be used to extract valuable information from the acquired AE signal.

Despite the promising results, there is a lot of room for improvement. All analysis of the AE signal strongly depends on the detection of clusters or evolving paths in the intensity images. For this reason, different signal and image processing techniques need to be investigated at

each step, from subband filtering to feature extraction, and from feature extraction to the generation of the 3D surfaces and/or intensity images. The investigation should also include a further in-depth study of AE features, e.g. the effect of using different coding for the hit pattern feature or different pattern lengths.

Furthermore, automation is needed. The identification and selection of hit patterns for AE tracking was done manually through visual inspection of intensity images. It is unlikely that the same patterns will be useful for other test specimens. Furthermore, evolving paths only appear in certain intensity images, depending both on the type of feature and on the subband. Hence, in order to make both the method and the AE hit pattern feature attractable an automatic detection of paths and patterns in the intensity images is needed.

Finally, if one wishes to use a reference signal other than relative time, e.g. load or displacement, then the methodology must be augmented to handle reference signals with both a variable rate and changing dynamic range.

7. Acknowledgements

The author wishes to thank Össur hf. for both providing prosthetic feet for testing and access to their testing facilities. Furthermore, the author wants to acknowledge the financial support from the University of Iceland Research Fund, the Icelandic Research Council Research Fund, the Icelandic Research Council Graduate Research Fund and Landsvirkjun's Energy Research Fund.

8. References

Bohse, J. (2000). Acoustic emission characteristics of micro-failure processes in polymer blends and composites, *Composites Science and Technology* 60(8): 1213–1226.

Carlos, M. F. & Vallen, H. (2005). Acoustic Emission Signal Processing, *in* P. O. Moore (ed.), *Acoustic Emission Testing*, 3rd edn, Vol. 6 of *Nondestructive testing handbook*, American Society for Nondestructive Testing, Inc., Columbus, pp. 153–154.

De Groot, P. J., Wijnen, P. A. M. & Janssen, R. B. F. (1995). Real-time frequency determination of acoustic emission for different fracture mechanisms in carbon/epoxy composites, *Composites Science and Technology* 55(4): 405–412.

Degrieck, J. & Paepegem, W. V. (2001). Fatigue damage modeling of fibre-reinforced composite materials: Review, *Applied Mechanics Reviews* 54(4): 279–300.

Dixon, S., Pampalk, E. & Widmer, G. (2003). Classification of dance music by periodicity pattern, *International Symposium on Music Information Retrieval*, ISMIR.

Duesing, L. A. (1989). Acoustic emission testing of composite materials, *Reliability and Maintainability Symposium, 1989. Proceedings., Annual* pp. 128–134.

Dzenis, Y. A. & Qian, J. (2001). Analysis of microdamage evolution histories in composites, *International Journal of Solids and Structures* 38(10-13): 1831–1854.

Giordano, M., Calabro, A., Esposito, C., D'Amore, A. & Nicolais, L. (1998). An acoustic-emission characterization of the failure modes in polymer-composite materials, *Composites Science and Technology* 58(12): 1923–1928.

Green, E. R. (1998). Acoustic emission in composite laminates, *Journal of Nondestructive Evaluation* 17(3): 117–127.

Halverson, H. G., Curtin, W. A. & Reifsnider, K. L. (1997). Fatigue life of individual composite specimens based on intrinsic fatigue behavior, *International Journal of Fatigue* 19(5): 369–377.

Hellier, C. J. (2001). *Handbook of Nondestructive Evaluation*, McGraw-Hill, New York.

Iwamoto, M., Ni, Q.-Q., Fujiwara, T. & Kurashiki, K. (1999). Intralaminar fracture mechanism in unidirectional CFRP composites: Part I: Intralaminar toughness and AE characteristics, *Engineering Fracture Mechanics* 64(6): 721–745.

Kamala, G., Hashemi, J. & Barhorst, A. A. (2001). Discrete-Wavelet Analysis of Acoustic Emissions During Fatigue Loading of Carbon Fiber Reinforced Composites, *Journal of Reinforced Plastics and Composites* 20(3): 222–238.

Mercer, C. A. (2001). Removing phase delay using phaseless filtering - a phaseless filtering technique that eliminates time lag. http://www.prosig.com/signal-processing/PhaselessFiltering.html.

Mouritz, A. P. (2003). Non-destructive evalutation of damage accumulation, *in* B. Harris (ed.), *Fatigue in Composites*, Woodhead Publishing Ltd., Cambridge, pp. 242–266.

Nayeb-Hashemi, H., Kasomino, P. & Saniei, N. (1999). Nondestructive evaluation of fiberglass reinforced plastic subjected to combined localized heat damage and fatigue damage using acoustic emission, *Journal of Nondestructive Evaluation* 18(4): 127–137.

Olson, H. F. (1967). *Music, Physics and Engineering*, 2nd ed. edn, Dover Publications, New York.

Prosser, W. H. (1996). Applications of Advanced Waveform-Based AE Techniques for Testing Composite Materials, *Proceedings of the SPIE conference on Nondestructive Evaluation Techniques for Aging Infrastructure and Manufacturing: Materials and Composites*, Scottsdale, Arizona, pp. 146–153.

Prosser, W. H., Jackson, K. E., Kellas, S., Smith, B. T., McKeon, J. & Friedman, A. (1997). Advanced waveform-based acoustic emission detection of matrix cracking in composites, *NDT and E International* 30(2): 108.

Rieke, F., Warland, D., de Ruyter van Steveninck, R. & Bialek, W. (1997). *Spikes: Exploring the Neural Code*, Computational Neuroscience, The MIT Press.

Sethares, W. A., Morris, R. D. & Sethares, J. C. (2005). Beat tracking of musical performances using low-level audio features, *Speech and Audio Processing, IEEE Transactions on* 13(2): 275–285.

Tsamtsakis, D., Wevers, M. & De Meester, P. (1998). Acoustic Emission from CFRP Laminates During Fatigue Loading, *Journal of Reinforced Plastics and Composites* 17(13): 1185–1201.

Unnthorsson, R. (2008). *Acoustic Emission Monitoring of CFRP Laminated Composites Subjected to Multi-axial Cyclic Loading*, Ph.D. dissertation, University of Iceland.

Unnthorsson, R., Pontoppidan, N. H. & Jonsson, M. T. (2005). Extracting Information from Conventional AE Features for Fatigue onset Damage Detection in Carbon Fiber Composites, *The 59th meeting of the Society for Machinery Failure Prevention Technology*, Society for Machinery Failure Prevention Technology, Virginia Beach, USA, pp. 293–302.

Unnthorsson, R., Runarsson, T. P. & Jonsson, M. T. (2007a). Monitoring The Evolution of Individual AE Sources In Cyclically Loaded FRP Composites, *Journal of Acoustic Emission* 25(January-December): 253–259.

Unnthorsson, R., Runarsson, T. P. & Jonsson, M. T. (2007b). On Using AE Hit Patterns for Monitoring Cyclically Loaded CFRP, *Journal of Acoustic Emission* 25(January-December): 260–266.

Unnthorsson, R., Runarsson, T. P. & Jonsson, M. T. (2008a). Acoustic Emission Based Fatigue Failure Criterion for CFRP, *International Journal of Fatigue* 30(1): 11–20. doi:10.1016/j.ijfatigue.2007.02.024.

Unnthorsson, R., Runarsson, T. P. & Jonsson, M. T. (2008b). AE Feature for Early Failure Warning of CFRP Composites Subjected to Cyclic Fatigue, *Journal of Acoustic Emission* 26(January-December): 229–239.

Wevers, M. (1997). Listening to the sound of materials: acoustic emission for the analysis of material behaviour, *NDT and E International* 30(2): 99–106.

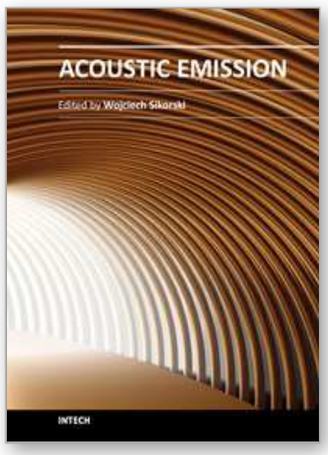

Acoustic Emission

Edited by Dr. Wojciech Sikorski

ISBN 978-953-51-0056-0
Hard cover, 398 pages
Publisher InTech
Published online 02, March, 2012
Published in print edition March, 2012

Acoustic emission (AE) is one of the most important non-destructive testing (NDT) methods for materials, constructions and machines. Acoustic emission is defined as the transient elastic energy that is spontaneously released when materials undergo deformation, fracture, or both. This interdisciplinary book consists of 17 chapters, which widely discuss the most important applications of AE method as machinery and civil structures condition assessment, fatigue and fracture materials research, detection of material defects and deformations, diagnostics of cutting tools and machine cutting process, monitoring of stress and ageing in materials, research, chemical reactions and phase transitions research, and earthquake prediction.

How to reference

In order to correctly reference this scholarly work, feel free to copy and paste the following:

Rúnar Unnþórsson (2012). Identifying and Monitoring Evolving AE Sources, Acoustic Emission, Dr. Wojciech Sikorski (Ed.), ISBN: 978-953-51-0056-0, InTech, Available from: http://www.intechopen.com/books/acoustic-emission/identifying-and-monitoring-evolving-ae-sources

INTECH
open science | open minds

InTech Europe
University Campus STeP Ri
Slavka Krautzeka 83/A
51000 Rijeka, Croatia
Phone: +385 (51) 770 447
Fax: +385 (51) 686 166
www.intechopen.com

InTech China
Unit 405, Office Block, Hotel Equatorial Shanghai
No.65, Yan An Road (West), Shanghai, 200040, China
中国上海市延安西路65号上海国际贵都大饭店办公楼405单元
Phone: +86-21-62489820
Fax: +86-21-62489821

IntechOpen